Magnetic polarization effects of temperature sensors and heaters in LISA Pathfinder

J. Sanjuán,[1] A. Lobo,[1] M. Nofrarias,[1] N. Mateos,[1] X. Xirgu,[1] P. Cañizares,[1] and J. Ramos-Castro[2]
[1]*Institut de Ciències de l'Espai (CSIC-IEEC), Edifici Nexus, Gran Capità 2-4, 08034 Barcelona, Spain*
[2]*Departament d'Enginyeria Electrònica, Universitat Politècnica de Catalunya (UPC), Edif. C4, Jordi Girona 1-3, 08034 Barcelona, Spain*

(Received 28 April 2008; accepted 15 July 2008; published online 14 August 2008)

Temperature sensors and heaters belong in the diagnostics subsystem of the LISA Technology Package (LTP) on board LISA Pathfinder, the technology demonstrator for LISA. A number of these diagnostics items are placed at short distances from the LTP proof masses and are negative temperature coefficient (NTC) thermistors. By design, these devices have tiny amounts of ferromagnetic materials, which therefore constitute a potential source of disturbance to the performance of the LTP. In this paper we report on detailed magnetic characterization of the NTCs and use the data to evaluate their impact on the acceleration noise budget of the LTP. The effect is seen to be small if the NTCs are submitted to a demagnetization process before they are attached. Remagnetization is unlikely, as rather strong fields (approximately millitesla) are required to produce enough NTC magnetic polarization. © *2008 American Institute of Physics.*
[DOI: 10.1063/1.2968113]

I. INTRODUCTION

LISA Pathfinder (LPF) is an ESA mission, with NASA contributions, whose objectives are to put to test a number of critical parts of LISA [Laser Interferometer Space Antenna, the first space-borne gravitational wave (GW) detector]. Some of these parts are expected to make it directly into LISA.[1] The science module on board LPF is the LISA Technology Package (LTP).

One of the main purposes of the LTP is to demonstrate the possibility of keeping two test masses (TMs) in pure geodesic motion (free fall) to a given level of accuracy. Nominal free fall is of course the main concept behind GW detection science:[2] indeed, the detection principle for LISA is to measure the GW induced relative accelerations (*geodesic deviation*) of two TMs freely falling in the background gravitational field. The weakness of GWs imposes serious constraints on the level of accuracy to which free fall must be guaranteed in order to actually resolve the GW signal. In particular, because LISA is a space instrument, there are various spurious agents (e.g., solar wind), which would drive free-flying TMs out of their purely gravity driven motion. The action of such disturbances must therefore be screened out, and this is done by means of the so-called *drag-free* subsystem: the proof masses are housed inside a spacecraft, which shields them from undesired external perturbations. In its interior, the proof masses freely float. A precision measurement system, consisting in a capacitive sensor and a laser interferometer,[3–5] is able to detect tiny relative displacements between spacecraft and proof mass, then sends signals to a system of spacecraft microthrusters that move the latter to restore the centered position of the test masses, which are thus safely kept in geodesic motion.

For LISA to reach its scientific goals,[6] a requirement is set on the level of accuracy to which TM free fall must be ensured. Since LPF is a precursor mission, that level has been relaxed by an order of magnitude relative to that of LISA. The requirement is customarily expressed in terms of a spectral density of TM *relative acceleration* noise, and it is

$$S_{\Delta a,\mathrm{LPF}}^{1/2}(\omega) \leqslant 3 \times 10^{-14}\left[1+\left(\frac{\omega/2\pi}{3\ \mathrm{mHz}}\right)^2\right]\mathrm{m\ s^{-2}\ Hz^{-1/2}}, \tag{1}$$

which must apply within the LTP frequency band 1 mHz $\leqslant \omega/2\pi \leqslant$ 30 mHz. This is a truly demanding requirement, which imposes stringent limitations on tolerable instrumental noise and on *internal* environmental fluctuations within the LTP, such as temperature and magnetic field fluctuations. The latter are derived from the above top level requirement [Eq. (1)] by suitable apportioning criteria.[7] Even if environmental stability conditions are met, precision thermal and magnetic measurements are necessary to evaluate and properly understand the origin of their actual fluctuations. To this effect, the diagnostic subsystem is set up in the LTP.[8] It basically consists in sets of sensors, plus controlled disturbance generators for calibration purposes.

The thermal diagnostic subsystem accordingly consists of 24 temperature sensors and 14 control heaters, strategically distributed across the LTP.[9,10] Temperature sensors are negative temperature coefficient (NTC) thermistors, and heaters vary according to placement in the LTP. A number of temperature sensors and heaters are attached to the outer faces of the electrode housing (EH) surrounding the TMs. More specifically, two sensors and two heaters on each of the two EH face perpendicular to the LTP sensitive axis. All in all, eight devices are laid down around each of the TMs, a distance of only ~13 millimeters away—see Fig. 1.

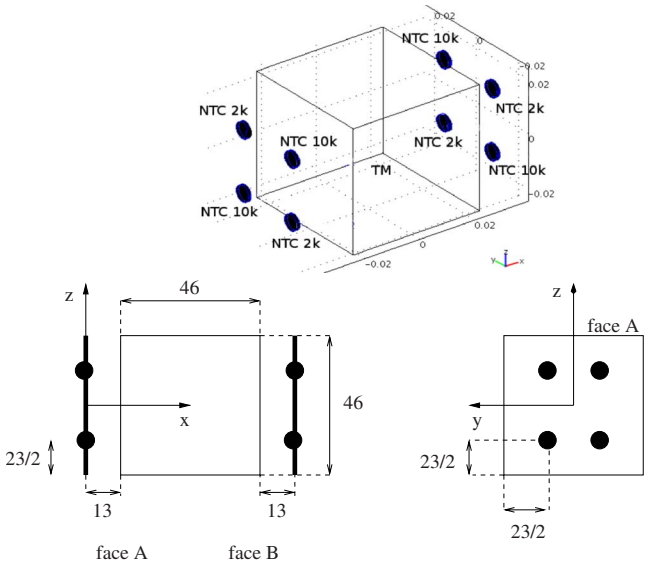

FIG. 1. (Color online) Layout of the eight NTCs in the EH (the TMs are located inside the EH) around one TM. Axes are labeled with distances in millimeters. The approximate distance of each thermistor to the TM is 13 mm, as shown in the bottom plots. NTCs are attached to the electrodes surrounding the TMs but have been omitted in the figure for clarity.

These diagnostic items are all NTCs: 10 and 2 kΩ nominal resistance thermistors for sensors and heaters, respectively. Thermistors were chosen as temperature sensors due to the strong dependence of their Ohmic resistance on temperature variations. Outgassing limit requirements inside the LTP vacuum enclosure was the reason for also using thermistors as heaters in this case. NTCs however are manufactured by mixing and synthesizing oxides doped with metals, such as manganese, nickel, cobalt, iron, and copper.[11] Except manganese and copper, which show paramagnetic and diamagnetic behaviors, respectively, these materials show ferromagnetic behavior. In spite of their tiny size, NTC magnetic properties can jeopardize the performance of the LTP, as they are placed quite near the TMs—see Fig. 1. The thermistors intended to be used in the LTP are BetaTherm thermistors, specifically, G10K4D and G2K7D models.[12]

Magnetic cleanliness in the LTP must comply with requirements that limit the acceptable values of magnetic field and gradient in the region occupied by the TMs. These requirements are set both for dc values and fluctuations of those quantities—see Sec. II. Previous experiments—such as the Advanced Composition Explorer[13] currently measuring the magnetic field in the Lagrange point L1, where LPF will also operate—have shown that the interplanetary magnetic field will not pose a problem in this sense since its dc values and fluctuations are orders of magnitude below the LTP magnetic requirements—see Table 2. We thus only need to consider the magnetic field generated by the sources *inside* the LPF spacecraft and, among these, specially those that are close to the TM, i.e., the thermistors.

All magnetic sources will be outside the LTP Core Assembly (LCA) and are designed not to exceed the magnetic requirements in the TM location. Inside the LCA, only thermal diagnostic items will be close enough to perturb the magnetic cleanliness, in case of being magnetically active. The noise acceleration budget assigned to magnetic effects has been set to[7]

$$S^{1/2}_{\Delta a,\mathrm{magnetic}}(\omega) \leqslant 12 \times 10^{-15}\ \mathrm{m\ s^{-2}\ Hz^{-1/2}} \tag{2}$$

in the measurement bandwidth (MBW) of the LTP.

This paper addresses the problem of the potential excess noise caused by the possible magnetic behavior of NTC thermistors in the LTP. It is organized as follows: in Sec. II we review the mechanism whereby magnetic fields induce forces in the TM, which result in the expression given by Eq. (9) in terms of the power spectral density (PSD). In Sec. III, we present the measurements performed to characterize magnetically the NTC thermistors and the relationships between the magnetic moment of the thermistors and the magnetic field and magnetic field gradient—Eqs. (11) and (12). BetaTherm and YSI thermistors have been characterized for comparison. In Sec. IV we estimate the effect of the NTC thermistors in the TM noise acceleration, and Sec. V summarizes our conclusions and actions to minimize the risk of acceleration noise in the TM due to the thermistors.

II. FORCE FLUCTUATIONS IN THE TM DUE TO MAGNETIC FIELD AND MAGNETIC FIELD GRADIENT

If a magnetic field $\mathbf{B}$ acts on a small volume d^3x of magnetic material with low magnetic susceptibility χ and density of magnetic moment $\mathbf{M}$, then the force on that small volume is given by[14]

$$\frac{d\mathbf{F}}{d^3x} = \boldsymbol{\nabla}\left[\left(\mathbf{M} + \frac{\chi}{2\mu_0}\mathbf{B}\right)\cdot\mathbf{B}\right] = \left[\left(\mathbf{M} + \frac{\chi}{\mu_0}\mathbf{B}\right)\cdot\boldsymbol{\nabla}\right]\mathbf{B}, \tag{3}$$

where $\mu_0 = 4\pi \times 10^{-7}\ \mathrm{m\ kg\ s^{-2}\ A^{-2}}$ is the magnetic constant. The right hand side equation follows from the first as a consequence of Maxwell's equation $\boldsymbol{\nabla}\times\mathbf{B}=0$.

To calculate the total force on the TM, Eq. (3) must be integrated to its volume V, which is $V=(46\ \mathrm{mm})^3$. It is expedient to express the integral in terms of averaged quantities defined by

$$\langle f\rangle \equiv V^{-1}\int_V f(x)d^3x, \tag{4}$$

where f is any function, scalar, vector, or tensor. We are mostly interested in the x-component of the force, as it is the relevant one for the mission science. With this notation,

$$F_x = V\langle \mathbf{M}\cdot\nabla B_x\rangle + \frac{\chi V}{\mu_0}\langle \mathbf{B}\cdot\boldsymbol{\nabla}B_x\rangle. \tag{5}$$

The *fluctuations* of the force are, from Eq. (5), given by

$$\delta F_x = V\langle \delta\mathbf{M}\cdot\boldsymbol{\nabla}B_x\rangle + V\langle \mathbf{M}\cdot\delta(\boldsymbol{\nabla}B_x)\rangle + \frac{\chi V}{\mu_0}\langle \delta\mathbf{B}\cdot\boldsymbol{\nabla}B_x\rangle + \frac{\chi V}{\mu_0}\langle \mathbf{B}\cdot\delta(\boldsymbol{\nabla}B_x)\rangle, \tag{6}$$

where δ refers to *temporal fluctuations*, and provided second order terms are neglected.[15]

The magnetic field $\mathbf{B}$ in Eq. (6) is the sum of the background field $\mathbf{B}_{\mathrm{bg}}$ and the field created by the NTC thermistors, if any, $\mathbf{B}_{\mathrm{NTC}}$,

TABLE I. TM magnetic properties (Ref. 7).

$\lvert\chi\rvert$	$\lvert\mathbf{M}\rvert$	$S_{\mathbf{M}}(\omega)$
10^{-5}	10^{-4} A m^{-1}	$\simeq 0$

$$\mathbf{B} = \mathbf{B}_{\mathrm{bg}} + \mathbf{B}_{\mathrm{NTC}}. \tag{7}$$

Fluctuations of the density of magnetic moment of the TM, $\delta\mathbf{M}$, can be neglected since the environmental temperature is extremely stable.[16] As regards the NTCs, the magnetic moment fluctuation needed to reach the background magnetic field fluctuations is around 100 μA m^2—use Eq. (11)—which is physically unfeasible as it is higher than the saturation moment—see Table IV. Consequently, Eq. (6) can be simplified to

$$\delta F_x = V\langle \mathbf{M}\cdot\delta(\nabla B_x)\rangle + \frac{\chi V}{\mu_0}\langle \delta\mathbf{B}\cdot\nabla B_x\rangle + \frac{\chi V}{\mu_0}\langle \mathbf{B}\cdot\delta(\nabla B_x)\rangle, \tag{8}$$

where $\delta\mathbf{B}$ and $\delta(\nabla B_x)$ refer only to the background magnetic field.

A worst case estimate of the force fluctuations in the TM (in terms of spectral density) due to the magnetic properties of the TM and the magnetic field and magnetic field gradient in it is (see the Appendix)

$$S_{\delta F_x}(\omega) = V^2|\langle\mathbf{M}\rangle|^2 S_{\nabla B_x}(\omega) + \left(\frac{\chi V}{\mu_0}\right)^2 |\langle\nabla B_x\rangle|^2 S_{\mathbf{B}}(\omega) + \left(\frac{\chi V}{\mu_0}\right)^2 |\langle\mathbf{B}\rangle|^2 S_{\nabla B_x}(\omega), \tag{9}$$

where $S(\omega)$ refers to the PSD. The values of $S_{\mathbf{B}}$ and $S_{\nabla B_x}$ are assumed uniform throughout the TM volume. This approach is again based on the assumption that fluctuations come only from the background field which can be considered *homogeneous* in the TM volume. The same applies to its fluctuations—see Table II.

From Eq. (9) it can be noticed that the potential *excess* noise due to the presence of the NTCs surrounding the TM will only come from the last two terms since the first term is only affected by the magnetic field gradient background fluctuations, $S_{\nabla B_x}$, and the density of magnetic moment of the TM, $\mathbf{M}$. Numerical evaluation of Eq. (9) depends on the values of the fluctuations of the environmental magnetic field and gradient, as dc magnetic fields couple to fluctuating fields to generate *noise* due to the non-null magnetic susceptibility χ of the TMs. The magnetic properties of the TM are given in Table I. Environmental magnetic field requirements are shown in Table II. The measurement and estimation of the averaged values in Eq. (9) caused by the presence of the NTCs, $|\langle\mathbf{B}_{\mathrm{NTCs}}\rangle|$ and $|\langle\nabla B_{\mathrm{NTCs}}\rangle|$, are detailed in Sec. III, while the dc values $\mathbf{B}_{\mathrm{bg}}$ and $\nabla B_{\mathrm{bg},x}$ are given in Table II.

TABLE II. Magnetic dc requirements in the TMs location (Ref. 7) and estimated magnetic fluctuations in the TM location (Ref. 24). Note that $S^{1/2}_{\mathbf{B}} = S^{1/2}_{\mathbf{B}_{\mathrm{bg}}}$ and $S^{1/2}_{\nabla B_x} = S^{1/2}_{\nabla B_{\mathrm{bg},x}}$ since the magnetic field background and its gradient are the only time dependent terms.

dc req.	PSD est. $\forall\mathbf{x}$
$\lvert\mathbf{B}_{\mathrm{bg}}\rvert \leqslant 10$ μT	$S^{1/2}_{\mathbf{B}}(\omega) \leqslant 650$ nT Hz$^{-1/2}$
$\lvert\nabla B_{\mathrm{bg},x}\rvert \leqslant 5\sqrt{3}$ μT m^{-1}	$S^{1/2}_{\nabla B_x}(\omega) \leqslant 250\sqrt{3}$ nT m^{-1} Hz$^{-1/2}$

TABLE III. Nominal (in the absence of NTCs) noise values in terms of force and acceleration ($m_{\mathbf{TM}} = 1.96$ kg) within the MBW.

Term	$S_{\delta F_x}$ (fN Hz$^{-1/2}$)	$S_{\Delta a_x}$ (fm s^{-2} Hz$^{-1/2}$)
$V\lvert\langle\mathbf{M}\rangle\rvert S^{1/2}_{\nabla B_x}(\omega)$	4.21	2.15
$(\chi V/\mu_0)\lvert\langle\nabla B_x\rangle\rvert S^{1/2}_{\mathbf{B}}(\omega)$	4.35	2.22
$(\chi V/\mu_0)\lvert\langle\mathbf{B}\rangle\rvert S^{1/2}_{\nabla B_x}(\omega)$	3.34	1.70
$S^{1/2}_{\mathrm{total\ mag}}(\omega)$	8.73	4.46

The numbers shown in Tables I and II yield a *nominal* acceleration noise due to magnetic effects in the TM in the absence of thermistors, i.e., $\mathbf{B} = \mathbf{B}_{\mathrm{bg}}$ and $\nabla B_x = \nabla B_{\mathrm{bg},x}$. The values are given in Table III, which will be the noise reference when considering the force noise added by the magnetization of the thermistors. The last row in the table is the total magnetic noise spectral density and is evaluated by the expression

$$S^{1/2}_{\mathrm{total\ mag}}(\omega) = V\left[\left(\frac{\chi}{\mu_0}|\langle\nabla B_x\rangle\right)^2 S_{\mathbf{B}}(\omega) + \left(|\langle\mathbf{M}\rangle| + \frac{\chi}{\mu_0}|\langle\mathbf{B}\rangle|\right)^2 S_{\nabla B_x}(\omega)\right]^{1/2}. \tag{10}$$

It is thus clear that the requirement set in Eq. (2) is comfortably satisfied in this scenario.

III. MAGNETIC FIELD AND MAGNETIC FIELD GRADIENT IN THE TM DUE TO NTCS: MEASUREMENT OF THE MAGNETIC PROPERTIES OF THE NTCS

G10K4D and G2K7D BetaTherm NTCs are small devices, 6 mm in diameter and 2 mm thick, which result on a volume of $\sim$40 nm^3.[12] Eight NTCs surround each of the TMs at a distance of $\simeq$13 mm as shown in Fig. 1.

In the following, in order to estimate the magnetic field and magnetic field gradient provoked by the thermistors in the TM, we shall make the assumption that the NTCs behave like magnetic dipoles of remanent magnetic moments $\mathbf{m}_a$, $a = 1,\ldots,8$. Given their tiny size, corrections to this hypothesis may only be small. Under this assumption, the magnetic field created by these dipoles will be given by[14]

$$\mathbf{B}_{\mathrm{NTC}}(\mathbf{x}) = \frac{\mu_0}{4\pi}\sum_{a=1}^{8}\frac{3(\mathbf{m}_a\cdot\mathbf{n}_a)\mathbf{n}_a - \mathbf{m}_a}{|\mathbf{x}-\mathbf{x}_a|^3}, \tag{11}$$

and its gradient by

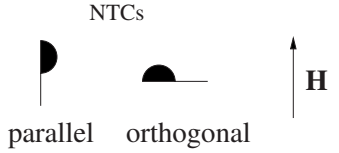

FIG. 2. Orientation configurations inside the SQUID with respect to the applied external magnetic field $\mathbf{H}$ for the NTC magnetic moment measurement.

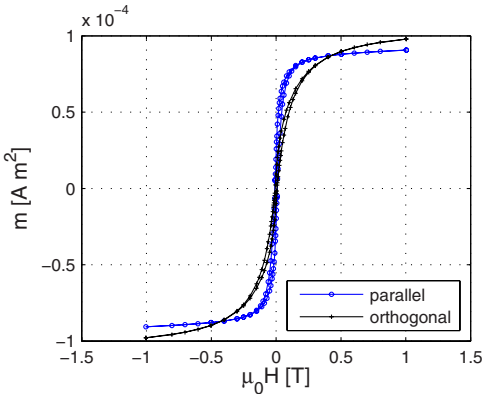

FIG. 3. (Color online) Hysteresis curve at 300 K for the 10 kΩ BetaTherm NTC thermistor.

$$\frac{\partial B_{\mathrm{NTC},i}}{\partial x_j} = \frac{\mu_0}{4\pi}\sum_{a=1}^{8}\frac{3}{|\mathbf{x}-\mathbf{x}_a|^4}[(m_{a,i}n_{a,j}+m_{a,j}n_{a,i})+(\mathbf{m}_a\cdot\mathbf{n}_a) \times(\delta_{ij}-5n_{a,i}n_{a,j})], \quad (12)$$

where $\mathbf{x}_a$ is the position of the ath NTC, and $\mathbf{n}_a$ is the unit vector in the direction from the ath NTC to the field point $\mathbf{x}$, or $\mathbf{n}_a=(\mathbf{x}-\mathbf{x}_a)/|\mathbf{x}-\mathbf{x}_a|$. δ_{ij} is the usual Kronecker symbol.

In order to evaluate Eqs. (11) and (12) and thus be able to calculate $|\langle\mathbf{B}_{\mathrm{NTC}}\rangle|$ and $|\langle\nabla B_{\mathrm{NTC},x}\rangle|$, we need to know the magnetic moments of the NTCs, $\mathbf{m}_a$. In the following sections we describe the measurements done to characterize magnetically the NTCs.

A. NTC magnetic characterization

The instrument used to characterize the magnetic properties of the thermistors is a magnetometer, specifically, a Quantum Design MPMS XL superconducting quantum interference device (SQUID) of the Serveis Científicotècnics of the Universitat de Barcelona. The tests consisted in measuring the magnetic moment **m** of the NTCs when subjected to an external magnetic field **H** and thus obtain the hysteresis cycle of the material. Moreover, in order to fully characterize the thermistor, the hysteresis curve was measured in two different orientations of the NTCs relative to the direction of the external field (configurations parallel and orthogonal)—see Fig. 2.

TABLE IV. BetaTherm (2 and 10 kΩ) NTC magnetic properties. Coercitive field $|\mu_0\mathbf{H}_{\mathrm{coer.}}|$ for both sensors and configurations is 10 mT.

Conf.	$\lvert\mathbf{m}_r\rvert_{2\ \mathrm{k\Omega}}$ (μA m^2)	$\lvert\mathbf{m}_{\mathrm{sat.}}\rvert_{2\ \mathrm{k\Omega}}$ (μA m^2)	$\lvert\mathbf{m}_r\rvert_{10\ \mathrm{k\Omega}}$ (μA m^2)	$\lvert\mathbf{m}_{\mathrm{sat.}}\rvert_{10\mathrm{k\Omega}}$ (μA m^2)
Par.	16	50	26	90
Orth.	7	50	9.4	100

We first characterized a BetaTherm 10 kΩ NTC (intended to be used as a temperature sensor) and a BetaTherm 2 kΩ NTC (intended to be used as a heater in the EH). The results are given in Figs. 3 and 4 for the 10 kΩ NTCs and the 2 kΩ NTCs, respectively. All the measurements were done at 300 K since this is the expected temperature at the TM location.

Results given in Figs. 3 and 4 show that both items exhibit a ferromagnetic behavior (the coercive field $\mu_0|\mathbf{H}_{\mathrm{coer}}|$ is about 10 mT) and that the remanent magnetic moment $\mathbf{m}_r$ of the 10 kΩ NTC is slightly higher than that of the 2 kΩ one. Table IV summarizes these results. The values of the remanent magnetic moment $\mathbf{m}_r$ are indicative of the very worst case since they reflect the magnetization of the sensor after being saturated. The saturating magnetic field is around 500 mT, a considerably large one.

The assessment of the effect of NTCs on the LTP acceleration noise depends on the quality of the determination of the magnetic properties of the thermistors, specially the remanent magnetic moment parameter $\mathbf{m}_r$. In view of this, measurements of a set of BetaTherm NTC thermistors (four samples) and another type of thermistor, YSI NTC (five samples of the YSI 44031 bead-type model[17]), were performed to ratify the parameters measured in Table IV and to compare them with another type of thermistor (the YSI one). Thermistors tested were all of 10 kΩ. NTCs of 2 kΩ were not tested because they are less *magnetic* than the 10 kΩ ones—see Table IV. Moreover, the magnetic moment of the BetaTherm thermistor was measured only for the parallel configuration since this corresponds to the worst case—see Table IV. The orientation in the YSI thermistors was irrelevant due to its spherical symmetry. Hysteresis curves for both sets of thermistors are shown in Figs. 5 and 6.

Figure 5 confirms the behavior observed in the measure-

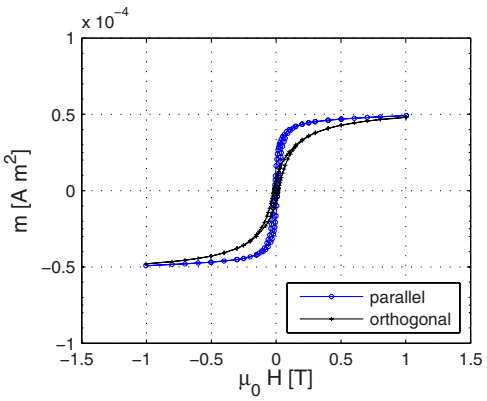

FIG. 4. (Color online) Hysteresis curve at 300 K for the 2 kΩ BetaTherm NTC thermistor.

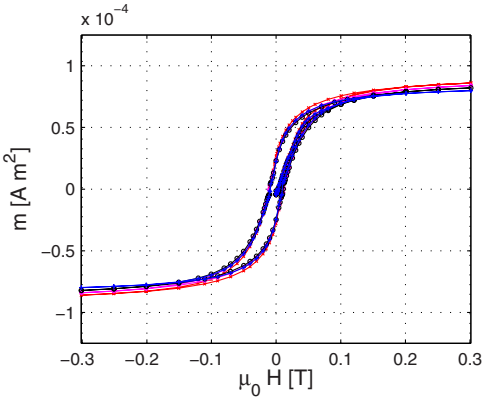

FIG. 5. (Color online) Hysteresis curve at 300 K for the set (four samples) of 10 kΩ NTC thermistors of BetaTherm and parallel configuration.

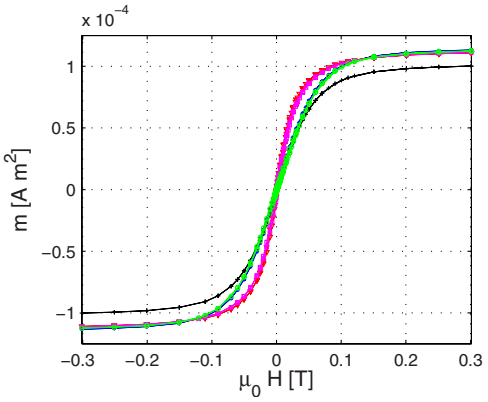

FIG. 6. (Color online) Hysteresis curve at 300 K for the set (five samples) of 10 kΩ YSI NTC thermistors.

ments done previously with the BetaTherm NTCs, i.e., ferromagnetism. However, Fig. 6 shows that YSI thermistors get easily demagnetized after removing the external magnetic field, i.e., they have a comparatively small coercive field ($\simeq$1 mT) and a small susceptibility, too. Finally, Figs. 5 and 6 show that the results for each set of thermistors are consistent with one another (small standard deviation values). Results are summarized in Table V.

B. Numerical calculations

In order to evaluate Eq. (9) we will first calculate the averaged values of the magnetic field and magnetic field gradient created by the NTCs—Eqs. (11) and (12). We will make the simplifying assumption that all eight NTCs are 10 kΩ, even if only four are. We will accordingly overestimate the magnetic effect, which gets us on the safe side.

The evaluation of the averaged values has been done by means of numerical methods. More specifically, by a finite element method approach: the volume of the TM $(46\ \text{mm})^3$ has been divided into N volume elements, ΔV $(=V/N)$, and for each ΔV Eqs. (11) and (12) have been used, then the average value and modulus calculated, i.e.,

$$\langle \mathbf{B}_{\text{NTC}} \rangle \simeq N^{-1} \sum_{k=1}^{N} \mathbf{B}_{\text{NTC}}(\mathbf{x}_k), \tag{13}$$

$$\langle \nabla B_{\text{NTC},x} \rangle \simeq N^{-1} \sum_{k=1}^{N} \nabla B_{\text{NTC},x}(\mathbf{x}_k), \tag{14}$$

where $\mathbf{x}_k$ is the position of the kth volume element. This has been chosen to be 8 mm^3, which corresponds to $N=12\,167$. Decreasing the size of the volume elements did not improve the results of the computations. Calculations considering different orientations of the eight magnetic moments of the NTCs allow us to know the worst possible magnetic moment orientation combinations for each axis. These are summarized in the four configurations shown in Fig. 7. In terms of magnetic field, configurations B and D give the highest mean magnetic field values. However, the magnetic field gradient is zero. On the contrary, configurations A and C yield the highest mean values of the magnetic field gradient, but the mean magnetic field is zero. Intermediate configurations have been seen to produce milder effects. The results obtained for the configurations given in Fig. 7 are summarized in Table VI, and they can be seen graphically for configurations A and B in Figs. 8 and 9, respectively.

TABLE V. Magnetic properties for the two sets of thermistors tested. BetaTherm values are for the parallel configuration (see Fig. 2) and for 10 kΩ of nominal resistance only. Four BetaTherm samples and five YSI samples were measured.

Sensor	$\lvert\mathbf{m}_r\rvert$ (μA m^2)	$\lvert\mathbf{m}_{\text{sat.}}\rvert$ (μA m^2)	$\lvert\mu_0\mathbf{H}_{\text{coer.}}\rvert$ (mT)
BetaTherm	24 ± 2	83 ± 2.5	10
YSI	1.8 ± 0.5	110 ± 5	1

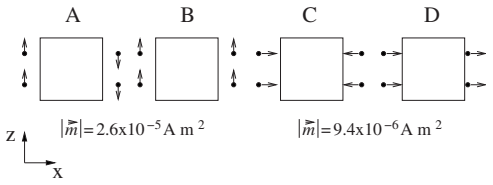

FIG. 7. Configurations analyzed for the evaluation of Eqs. (11) and (12). Configurations A and B assume the magnetic moments of all NTCs are oriented along the z-axis. However, in configuration A magnetic moments take opposite directions, while in B all the orientations are equal. Configurations C and D assume that all the NTCs are oriented along the x-axis. In configuration C magnetic moment orientations are opposite, while in configuration D all the orientations coincide. This four configurations cover the worst cases involved in the problem. The magnetic moment values used are extracted from Table IV.

C. NTC first magnetization curve

The magnetic moments used in the calculations of the previous section are remanent magnetic moments *after* saturating the NTCs. However, it must be realized that the magnetic fields in the environments the LTP will go through are orders of magnitude below the saturation field of the thermistor $\mu_0 H_{\text{sat}} \sim 500$ mT. For instance, the Earth magnetic field is in the order of 50 μT, the magnetic field in the van Allen belts is of the same order of magnitude,[18] and the interplanetary magnetic field is in the order of 10–100 nT.[19] These values suggest that we are heavily overestimating the effect of the NTCs on the TM when using the remanent magnetic moment after saturation, which fully magnetizes the device.[20]

To fine tune the previous estimates, we proceeded to analyze the first magnetization Curve (FMC) of the NTCs. The FMC is obtained by means of a two step procedure[21] (actually, it was already needed to determine the hysteresis curve in the previous measurements): (i) an alternating mag-

TABLE VI. Mean values and modulus for the magnetic field and magnetic field gradient caused by the eight NTCs in the TM. Magnetic moments used in configurations A and B are $\lvert\mathbf{m}_r\rvert=2.6$ μA m^2 and $\lvert\mathbf{m}_r\rvert=9.4$ μA m^2 for configurations C and D—see Table IV and Fig. 7.

Conf.	$\langle\mathbf{B}\rangle$; $\lvert\langle\mathbf{B}\rangle\rvert$ (μT)	$\langle\nabla B_x\rangle$; $\lvert\langle\nabla B_x\rangle\rvert$ (μT m^{-1})
A	(0,0,0); 0	(0,0,15.5); 15.5
B	(0,0,−0.25); 0.25	(0,0,0); 0
C	(0,0,0); 0	(−11.3,0,0); 11.3
D	(0.18,0,0); 0.18	(0,0,0); 0

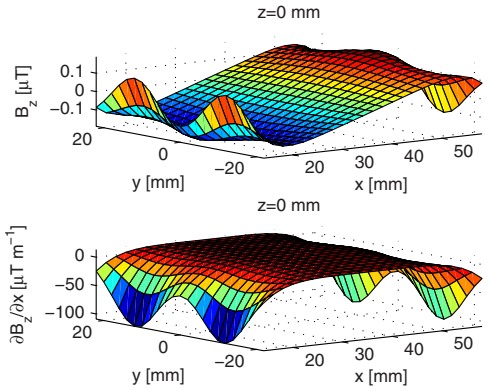

FIG. 8. (Color online) Configuration A (see Fig. 7) and $|\mathbf{m}|=26\ \mu\mathrm{A\ m}^2$. Representation of the z-component of the magnetic field and magnetic field gradient in the equatorial plane of the TM, i.e., xy-plane for $z=0$—see Fig. 1. The parity symmetries of field and gradient, $B_z(x,y)=B_z(x,-y)=-B_z(-x,y)$ and $\partial_x B_z(x,y)=\partial_x B_z(x,-y)=\partial_x B_z(-x,y)$, respectively, are clearly visible in the plots. In view of these symmetries, the field at the top averages to zero, while the gradient at the bottom does not (see Table VI for numerical values).

netic field with decreasing amplitude is applied to the sample in order to demagnetize it to the level of the instrument resolution, and (ii) an external magnetic field that slowly increases in small steps (~0.1 mT in our case) is applied to the sample. With this method, we first *erase* the magnetic moment of the NTC to then evaluate the *magnetic response* of the thermistor. We thus obtain the first response to the magnetic field, which will be lower than the response after applying a strong magnetic field. The FMC has been measured for the two sets of 10 kΩ NTC thermistors studied previously: the BetaTherm and the YSI ones. However, the demagnetization was only meaningful for the BetaTherm NTCs due to its ferromagnetic behavior, although not so for the YSI NTCs due to their narrow hysteresis curve—cf. Sec. III A. Results are shown in Figs. 10 and 11 and summarized in Table VII.

The FMC for the BetaTherm NTCs can be linearized near the full demagnetization zone. We find

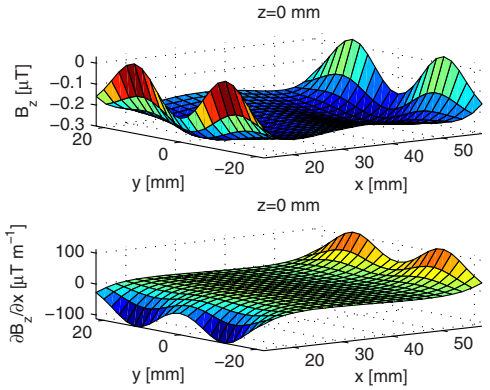

FIG. 9. (Color online) Configuration B (see Fig. 7) and $|\mathbf{m}|=26\ \mu\mathrm{A\ m}^2$. The same plots described in Fig. 8 are shown for configuration B. The parity symmetries of field and gradient are now slightly different, $B_z(x,y)=B_z(x,-y)=B_z(-x,y)$ and $\partial_x B_z(x,y)=\partial_x B_z(x,-y)=-\partial_x B_z(-x,y)$, and are also reflected in the plots. In view of these symmetries, the gradient at the bottom averages to zero, while the field at the top does not (see Table VI for numerical results).

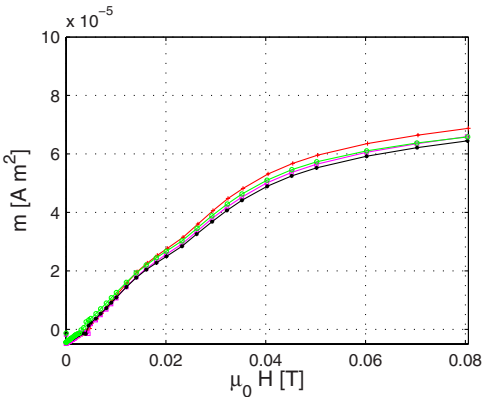

FIG. 10. (Color online) Measured FMC for the set of four BetaTherm samples (10 kΩ and parallel configuration).

$$|\mathbf{m}_{\mathrm{FMC,BetaTherm}}| \simeq 1.45\times 10^{-3}\mu_0|\mathbf{H}_{\mathrm{FMC}}|, \tag{15}$$

where international system units are used. This is very accurate up to magnetic fields of about 40 mT. However, because magnetization is not a reversible process, the above approximation cannot be used when it comes to estimate the remanent magnetization *after* the field which magnetized the NTC is switched off. It does however provide an *upper limit* of the magnetization remaining in the device, which corresponds to that reached when the field was on—see Fig. 12. Equation (15) will be useful to determine the maximum external magnetic field which the BetaTherm NTCs can tolerate, once the largest magnetic moment compatible with the TM magnetic acceleration noise budget is determined—see Sec. IV. Now we can recalculate Table VI with the magnetic moment after demagnetization and in the absence of background magnetic fields. Values obtained are given in Table VIII.

Values shown in Table VIII are all within the requirements given in Table II. Actually, the mean values of magnetic field and magnetic field gradient have been reduced by a factor of around 20 due to the magnetic moment reduction by a factor of 20 achieved with the demagnetization process.

IV. EXCESS TM NOISE CALCULATIONS

The results obtained in Secs. III B and III C can now be used to calculate the force/acceleration excess noise in the TM due to the presence of the thermistors. We only have to substitute the mean values of the magnetic field and mag-

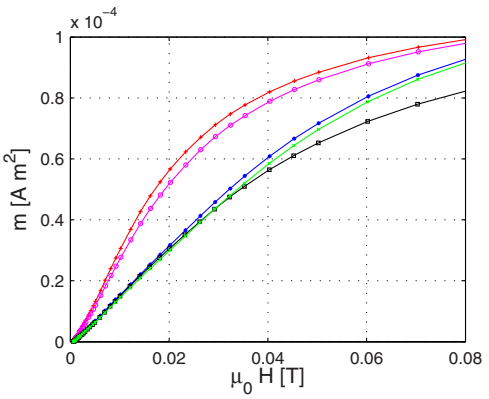

FIG. 11. (Color online) Measured FMC for the set of five YSI samples.

TABLE VII. Remanent magnetic moment after demagnetization $|\mathbf{m}_{\text{demag}}|$.

Sensor	$\lvert\mathbf{m}_{\text{demag}}\rvert$ (μA m^2)
BetaTherm (10 kΩ)	1.4 ± 0.2
YSI	0.75 ± 0.06

netic field gradient into Eq. (9). Calculations are given in Table IX for the BetaTherm thermistors and in Table X for the YSIs using the magnetic moment for the worst case (NTCs fully magnetized) and for the best case (NTCs fully demagnetized) for both thermistor sets.

The excess noise Δ is defined by

$$\Delta \doteq \frac{S^{1/2}_{\text{total mag,NTCs}} - S^{1/2}_{\text{total mag,no NTCs}}}{S^{1/2}_{\text{total mag,no NTCs}}}, \tag{16}$$

and $S^{1/2}_{\text{total mag}}$ has been calculated using Eq. (10).

From Tables IX and X we can notice that in any case, the total required magnetic cleanliness is reached—see Eq. (2)—since the maximum acceleration noise is $14.3/1.96 = 7.3$ fm s^{-2} Hz$^{-1/2}$ (BetaTherm NTC in configuration A and $|\mathbf{m}_r| = 24$ μA m^2). BetaTherm thermistors in the very worst case increase the excess noise by a 64%, whereas the YSI NTCs in the very worst case add a mere 4% excess noise. When demagnetizing the thermistors, a clear improvement can be observed in the BetaTherm NTCs. This improvement is not observed in the YSI ones, as previously stated.

If the noise added by BetaTherm thermistors is required not to exceed 10% of the nominal one, then we can calculate the background magnetic field to which they can be exposed. A 10% increase of the nominal noise is (in the MBW)

$$S^{1/2}_{\delta F_x,10\%\ \text{increase}}(\omega) \leqslant 9.6\ \text{fN Hz}^{-1/2}, \tag{17}$$

which means that

$$|\langle \nabla B_{\text{NTC},x} \rangle| \leqslant 4\ \mu\text{T m}^{-1}. \tag{18}$$

From Eq. (18) we can now calculate the maximum magnetic moment permitted assuming configuration A (worst case scenario). This results in

$$|\mathbf{m}|_{\max} \leqslant 7\ \mu\text{A m}^2, \tag{19}$$

which, using Eq. (15), leads to

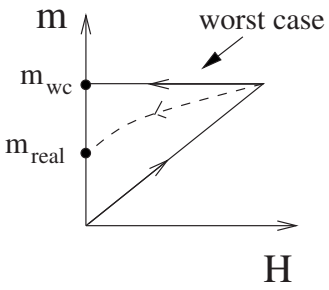

FIG. 12. Magnetic moment vs external magnetic field. After applying an external magnetic field, the remanent magnetic moment is $\mathbf{m}_{\text{WC}}$ in the very worst case assumption. $\mathbf{m}_{\text{real}}$ is a somewhat more realistic remanent magnetic moment.

TABLE VIII. dc values after demagnetization ($|\mathbf{m}_{\text{demag}}| = 1.4$ μA m^2) for the BetaTherm NTCs of 10 kΩ and for configurations A and B.

Conf.	$\langle \mathbf{B} \rangle$; $\lvert\langle \mathbf{B} \rangle\rvert$ (μT)	$\langle \nabla B_x \rangle$; $\lvert\langle \nabla B_x \rangle\rvert$ (μT m^{-1})
A	(0,0,0); 0	(0,0,0.84); 0.84
B	(0,0,0.01); 0.01	(0,0,0); 0

$$\mu_0 |\mathbf{H}|_{\max} \leqslant 5\ \text{mT}. \tag{20}$$

Consequently, in order to minimize the contribution of the NTCs to acceleration noise in the TMs, they should not be exposed to magnetic fields higher than 5 mT after having been demagnetized.

V. DISCUSSION

The work reported in the present paper originated from the observation that NTC thermistors, due to the materials they are made of, might constitute a problem potentially able to compromise the achievement of LPF's science output. The reason is that such materials have ferromagnetic properties, whereby they become so far unforeseen sources of magnetic field that contribute to increase the acceleration noise of the LTP proof masses. The proximity of some of the NTCs to the TMs was an additional element of risk for the optimum performance of the LTP. A quantitative study of the effects of the NTCs on the TMs was therefore mandatory, and the results have been presented here.

The study has revealed that under the most unfavorable conditions, very unlikely to be met in practice, the magnetic properties of the NTCs selected to fly in LPF can degrade the performance of the LTP, increasing the magnetic noise by ~65% relative to the background. Even in such extreme conditions the budgeted magnetic noise, 12 fm s^{-2} Hz$^{-1/2}$ (or 23.5 fN Hz$^{-1/2}$), is not reached—Table IX.

It also appears from the present study that demagnetization of the NTCs produces very good results: the magnetic noise they induce can be reduced by about an order of magnitude, which makes it mostly negligible. In addition, the strong fields required for magnetic saturation are as high as a fraction of a tesla, an extremely high field intensity that makes remagnetization an essentially impossible process in any LTP circumstances.[22]

For completeness, and as a backup, two families of NTC thermistors were subjected to the same analysis: one was manufactured by BetaTherm, and the other by YSI. The first had been chosen for flight before the magnetic issues were

TABLE IX. Force noise values for the BetaTherm (configuration A). Units in fN Hz$^{-1/2}$.

Term	No NTCs	$\lvert\mathbf{m}_r\rvert = 24$ μA m^2	$\lvert\mathbf{m}_{\text{demag}}\rvert = 1.4$ μA m^2
$V\lvert\langle M \rangle\rvert S^{1/2}_{\nabla B_x}(\omega)$	4.21	4.21	4.21
$\chi V/\mu_0 \lvert\langle \nabla B_x \rangle\rvert S^{1/2}_B(\omega)$	4.35	12	4.8
$\chi V/\mu_0 \lvert\langle B \rangle\rvert S^{1/2}_{\nabla B}(\omega)$	3.34	3.34	3.34
$S^{1/2}_{\text{total mag.}}(\omega)$	8.73	14.3	8.9
Δ	...	64%	2%

TABLE X. Force noise values for the YSI sensors (configuration A). Units in fN $Hz^{-1/2}$.

Term	No NTCs	$\lvert\mathbf{m}_r\rvert=1.8\ \mu$A m^2	$\lvert\mathbf{m}_{\text{demag}}\rvert=0.75\ \mu$A m^2
$V\lvert\langle M\rangle\rvert S^{1/2}_{\nabla B_{bg,x}}(\omega)$	4.21	4.21	4.21
$(\chi V/\mu_0)\lvert\langle\nabla B_x\rangle\rvert S^{1/2}_{B_{bg}}(\omega)$	4.35	4.9	4.6
$(\chi V/\mu_0)\lvert\langle B\rangle\rvert S^{1/2}_{\nabla B_{bg}}(\omega)$	3.34	3.34	3.34
$S^{1/2}_{\text{total mag.}}(\omega)$	8.73	9.1	8.85
Δ	⋯	4.2%	1.4%

spotted, while the second had been considered less convenient, on the basis of prior laboratory research work. It appears that the YSIs are significantly less magnetic than the BetaTherm's, and this translates into a milder contribution to the total noise when the former are used *without demagnetizing* them first. However, the differences when the NTCs are demagnetized basically disappear. The presumed stability of the demagnetized state in the BetaTherm's—see previous paragraph—thus confirms that the initial choice to fly this NTC brand should be maintained.

ACKNOWLEDGMENTS

We wish to thank Professor Amílcar Labarta, Universitat de Barcelona, for illuminating discussions and Núria Clos for her excellent work at the Serveis Científico-tècnics of the Universitat de Barcelona. Support for this work came from Project No. ESP2004-01647 of Plan Nacional del Espacio of the Spanish Ministry of Education and Science (MEC). J.S. acknowledges a grant from MEC, and M.N. from Generalitat de Catalunya.

APPENDIX: SPECTRAL DENSITY FUNCTION FOR THE FLUCTUATING FORCE

From

$$\delta F_x = V\langle \mathbf{M}\cdot\delta(\nabla B_x)\rangle + \frac{\chi V}{\mu_0}\langle \delta\mathbf{B}\cdot\nabla B_x\rangle + \frac{\chi V}{\mu_0}\langle \mathbf{B}\cdot\delta(\nabla B_x)\rangle, \tag{A1}$$

the PSD of the force fluctuations, i.e., $S_{\delta F_x}(\omega)$, is to be determined. For simplicity let us assume that Eq. (A1) is only

$$\delta F_x = V\langle \mathbf{M}\cdot\delta(\nabla B_x)\rangle. \tag{A2}$$

Now we assume that the temporal fluctuations of the magnetic field gradient, $\delta\nabla B_x$, are homogeneous across the TM volume, i.e.,

$$\delta F_x = V\langle \mathbf{M}\cdot\delta(\nabla B_x)\rangle = V\langle\mathbf{M}\rangle\cdot\delta(\nabla B_x). \tag{A3}$$

The spectral density function of Eq. (A3) is obtained by[23]

$$S_{\delta F_x}(\omega) = \frac{1}{2\pi}\int_{-\infty}^{\infty} R_{\delta F_x}(\tau)e^{-i\omega\tau}d\tau, \tag{A4}$$

where $R_{\delta F_x}(\tau)$ is the autocorrelation function of δF_x, i.e.,

$$R_{\delta F_x}(\tau) = \mathcal{E}\{\delta F_x(t)\,\delta F_x(t+\tau)\}. \tag{A5}$$

Here, $\mathcal{E}\{-\}$ is the expectation value operator. Substituting Eq. (A3) into Eq. (A5) and assuming that $\mathbf{M}$ is a time independent quantity, we obtain

$$R_{\delta F_x}(\tau) = V^2\mathcal{E}\left\{\sum_{i,j=1}^{3}\langle M_i\rangle\langle M_j\rangle\delta\left[\frac{\partial B_x(t)}{\partial x_i}\right]\delta\left[\frac{\partial B_x(t+\tau)}{\partial x_j}\right]\right\}. \tag{A6}$$

We now assume that cross terms in Eq. (A6) are uncorrelated and, consequently, cross terms in Eq. (A6) vanish,

$$R_{\delta F_x}(\tau) = V^2\mathcal{E}\left\{|\langle\mathbf{M}\rangle|^2\sum_{i=1}^{3}\delta\left[\frac{\partial B_x(t)}{\partial x_i}\right]\delta\left[\frac{\partial B_x(t+\tau)}{\partial x_i}\right]\right\}. \tag{A7}$$

Substituting Eq. (A7) into Eq. (A4), we obtain

$$S_{\delta F_x}(\omega) = V^2|\langle\mathbf{M}\rangle|^2\cdot S_{\nabla B_x}(\omega), \tag{A8}$$

assuming that fluctuations in the components of the field gradient are equal (in PSD) and uncorrelated or

$$S_{\partial B_x/\partial x_i} = S_{\partial B_x/\partial x}(\omega) \quad \text{for } i=1,2,3. \tag{A9}$$

Mutatis mutandi, we obtain the same expression for (i) the term $(\chi V/\mu_0)\langle\mathbf{B}\cdot\delta(\nabla B_x)\rangle$, where $\langle M\rangle$ is substituted by $\langle B\rangle$, and (ii) for the term $(\chi V/\mu_0)\langle\delta\mathbf{B}\cdot\nabla B_x\rangle$, where the constant term is $\langle\nabla B_x\rangle$ instead of $\langle\mathbf{M}\rangle$, and also assuming equality and uncorrelation of the fluctuations of the three components of the magnetic field,

$$S_{B_i}(\omega) = S_{B_x}(\omega) \quad \text{for } i=1,2,3. \tag{A10}$$

By linearly adding these spectral density functions, we obtain Eq. (9).

[1] D. Gerardi, W. Fichter, N. Brandt, C. Braxmaier, G. Heinzel, and S. Vitale, AIP Conf. Proc. **873**, 349 (2006).
[2] C. W. Misner, K. S. Thorne, and J. A. Wheeler, *Gravitation* (Freeman, San Francisco, 1973).
[3] S. Anza, M. Armano, E. Balaguer, M. Benedetti, C. Boatella, P. Bosetti, D. Bortoluzzi, N. Brandt, C. Braxmaier, M. Caldwell, L. Carbone, A. Cavalleri, A. Ciccolella, I. Cristofolini, M. Cruise, M. Da Lio, K. Danzmann, D. Desiderio, R. Dolesi, N. Dunbar, W. Fichter, C. Garcia, E. Garcia-Berro, A. Garcia-Marin, R. Gerndt, A. Gianolio, D. Giardini, R. Gruenagel, A. Hammesfahr, G. Heinzel, J. Hough, D. Hoyland, M. Hueller, O. Jenrich, U. Johann, S. Kemble, C. Killow, D. Kolbe, M. Landgraf, A. Lobo, V. Lorizzo, D. Mance, K. Middleton, F. Nappo, M. Nofrarias, G. Racca, J. Ramos, D. Robertson, M. Sallusti, M. Sandford, J. Sanjuan, P. Sarra, A. Selig, D. Shaul, D. Smart, M. Smit, L. Stagnaro, T. Sumner, C. Tirabassi, S. Tobin, S. Vitale, V. Wand, H. Ward, W. Weber, and P. Zweifel, Class. Quantum Grav. **22**, S125 (2005).
[4] G. Heinzel, V. Wand, A. Garcia, O. Jenrich, C. Braxmaier, D. Robertson, K. Middleton, D. Hoyland, A. Rudiger, R. Schilling, U. Johann, and K. Danzmann, Class. Quantum Grav. **21**, S581 (2004).
[5] D. Bortoluzzi, P. Bosetti, L. Carbone, A. Cavalleri, A. Ciccolella, M. Da Lio, K. Danzmann, R. Dolesi, A. Gianolio, G. Heinzel, D. Hoyland, C. D. Hoyle, M. Hueller, F. Nappo, M. Sallusti, P. Sarra, M. Te Plate, C. Tirabassi, S. Vitale, and W. Weber, Class. Quantum Grav. **20**, S89 (2003).
[6] A. Brillet, 25th Meeting of the IAU, Joint Discussion 1, Sydney Australia, 16–17 July 2003 (unpublished), Vol. 1.
[7] S. Vitale, LISA Pathfiner Report No. LTPA-UTN-ScRD-Iss003-Rev1, 2005.
[8] A. Lobo, M. Nofrarias, J. Ramos-Castro, J. Sanjuán, A. Conchillo, J. A. Ortega, X. Xirgu, H. Araujo, C. Boatella, M. Chmeissani , C. Grimani, C. Puigdengoles, P. Wass, E. Garcia-Berro, S. Garcia, L. Martinez, and G. Montero AIP Conf. Proc. **873**, 522 (2006).

[9] J. Sanjuán, J. Ramos-Castro, A. Lobo, M. Nofrarias, and P. J. Riu, Rev. Sci. Instrum. **78**, 104904 (2007).
[10] M. Nofrarias, A. F. García Marín, A. Lobo, G. Heinzel, J. Ramos-Castro, J. Sanjuán, and K. Danzmann, Class. Quantum Grav. **24**, 5103 (2007).
[11] R. Pallás and J. G. Webster, *Sensors and Signal Conditioning* (Wiley, New York, 2001).
[12] BetaTherm, www.betatherm.com
[13] Data extracted and analyzed from www.srl.caltech.edu/ACE/ASC/level2/lvl2DATA_MAG.html
[14] J. D. Jackson, *Classical Electrodynamics*, (Wiley, New York, 1998).
[15] Terms of the form $\delta\mathbf{B}\cdot\delta(\nabla B_x)$, etc. These may be relevant in the presence of high frequency fields which, due to the quadratic coupling, can generate low-frequency fluctuations. We do not consider this possibility here.
[16] A. Lobo, M. Nofrarias, J. Ramos-Castro, and J. Sanjuán, Class. Quantum Grav. **23**, 5177 (2006).
[17] YSI Temperature, www.meas-spec.com
[18] The mission CHAMP, http://www.gfz-potsdam.de/pb1/op/champ/results/index_RESULTS.html
[19] IEEC Report No. LTP-IEEC-1185-MagACEdata-2003.
[20] The highest risk of exposition to stronger fields actually resides in the *transport* phases of the LTP on ground when stronger magnets in transporting vehicle machinery may cause problems—see Sec. V.
[21] F. W. Sears and M. W. Zemansky, *College Physics* (Adison-Wesley, Reading, MA, 1991).
[22] L. Trougnou, personal communication (February 19, 2008).
[23] J. S. Bendat and A. G. Piersol, *Random Data* (Wiley, New York, 2000).
[24] S. Vitale, Document No. Unitn-Int/10-2002/Rel.1.3, 2002.